Editors' Suggestion

Simulation of memristive synapses and neuromorphic computing on a quantum computer

Ying Li
Graduate School of China Academy of Engineering Physics, Beijing 100193, China

(Received 14 May 2020; revised 24 October 2020; accepted 28 April 2021; published 26 May 2021)

One of the major approaches to spike-based neuromorphic computing is using memristors as analog synapses. We propose unitary quantum gates that exhibit memristive behaviors, including Ohm's law, pinched hysteresis loop and synaptic plasticity. Hysteresis depending on the quantum phase and long-term plasticity that encodes the quantum state are observed. We also propose a three-layer neural network with the capability of universal quantum computing. Quantum state classification on the memristive neural network is demonstrated. These results pave the way towards quantum spiking neural network built on unitary processes. We obtain these results in numerical simulations and experiments on the superconducting quantum computer *ibmq_vigo*.

DOI: 10.1103/PhysRevResearch.3.023146

I. INTRODUCTION

Neuromorphic computing is a brain-inspired computer paradigm in contrast with the von Neumann architecture [1,2]. According to the biological model of brain, information is stored and processed by a highly connected network formed of neurons, which provides the ability of learning, parallel and low energy cost computing, etc. Since the 1940s, it has been realized that how neurons wire up is essential [3]. Besides neuroscience, this observation also motives the development of computer programming, such as artificial neural network (ANN) vastly used in today's machine learning technologies [4,5]. In terms of the learning rule of neurons, spike-timing-dependent plasticity (STDP) is a biologically plausible model that has gained great attention in recent years [6–8]. In STDP, the synapse is strengthened or weakened depending on the temporal order between spikes of presynaptic and postsynaptic neurons [see Fig. 1(a)]. In this way, the brain can establish causal relationships between events.

Quantum computing uses quantum phenomena and is superior to classical computing in solving certain problems [9]. For example, to solve the integer factorization problem, Shor's quantum algorithm takes polynomial time with respect to the integer size, which is exponentially faster than the most efficient known classical algorithm [10]. In the circuit-based universal quantum computer, information is encoded in qubits and processed with unitary gates [11]. This kind of quantum machines is still under development but already demonstrates the power of surpassing classical computers [12,13]. Because the quantum computer for large-scale computing is not available yet, variational quantum algorithms are proposed for near-future applications [14–16]. Quantum neural networks are generalizations of classical ANN, in which unitary gates in the quantum circuit are taken as variables [17–26].

Memristor is a resistor with memory and one of the fundamental two-terminal circuit elements [see Fig. 1(b)] [27,28]. Its resistance decreases or increases depending on the input signal, i.e., voltage or current. Memristance can explain STDP in biological synapses [29]. Since the first memristive device was found in 2008 [30], the application as hardware analog of synapse in neuromorphic computing has been extensively investigated [2], mainly because memristive devices demonstrate behaviors similar to STDP [31,32]. Spiking neural networks [33,34] with the STDP learning rule are more biologically realistic than ANN such as sigmoid neurons [4,5], in which the computation is driven by spike events rather than the evaluation of differentiable functions.

In this paper, we propose memristorlike unitary quantum gates, see Fig. 1(c). These gates have the characteristic memristive property, i.e., hysteretic resistance state [28,30]. Given an oscillatory input state, the output-input observables display a pinched hysteresis loop. We find that this loop depends on not only the classical distribution but also the phase of input quantum state, which reflects the quantum nature of memristive gates. Using these gates to mimic synapses, we observe the long-term potentiation (LTP) and long-term depression (LTD), which are crucial for learning and memory in the neural network [6,8]. We show that quantum information can also be encoded in a manner similar to the long-term plasticity. Therefore, a spiking neural network built on memristive gates can process quantum information.

In addition to spiking neural network, memristive quantum gates can also be used to build a nonspiking quantum ANN. We propose a three-layer neural network taking parameters of memristive gates as variables, as shown in Fig. 1(d). Neurons in the input and hidden layers are qubits, and neurons in the output layer are classical bits. Two quantum layers are wired up by memristive gates, and output bits are measurement outcomes of hidden-layer qubits. Compared with the general quantum neural network [17], the number of variational parameters is significantly reduced with respect to the number

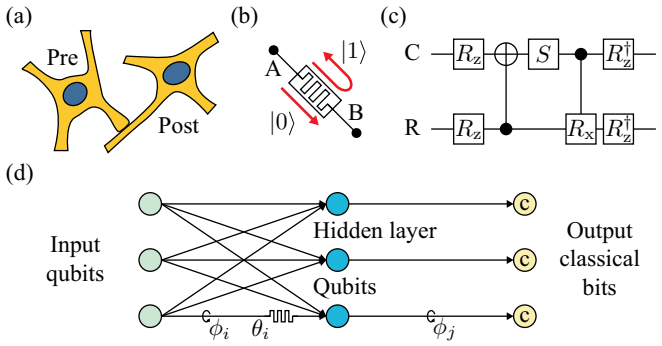

FIG. 1. (a) Presynaptic and postsynaptic biological neurons. (b) A memristor. In the quantum regime, we use qubits to represent the input/output current and resistance of the memristor. (c) Memristive gate M_θ decomposed into elementary quantum gates, where $R_z = e^{-i\frac{\theta}{2}Z}$ and $R_x = e^{-i(\frac{\pi}{2}-\theta)X}$. (d) Memristive quantum neural network.

of neurons and synapses. Each connection between an input neuron and a hidden-layer neuron is characterized by two variational parameters (i.e., weights), and each connection to an output neuron is characterized by only one parameter. We prove that such a three-layer memristive neural network is as powerful as a universal quantum computer [11] up to a polynomial overhead. The application of neural network is demonstrated in quantum state classification tasks [22–24,35].

All the results are demonstrated with numerical simulations using QuESTlink [36] and experiments on the quantum computer *ibmq_vigo*. The paper is organized as follows. In Sec. II, we give a brief review of the spiking neural network and STDP. In Sec. III, we introduce memristive quantum gates. Characteristic memristive properties, including pinched hysteresis loop and long-term plasticity, are discussed in Secs. IV, V, and VI. A protocol of quantum ANN built on memristive quantum gates is given in Sec. VII. In Sec. VIII, we discuss the universal quantum computing on the memristive ANN. Then, we demonstrate its application to the quantum state classification in Sec. IX. In Sec. X, we summarize and discuss the conclusions.

II. SPIKING NEURAL NETWORK AND STDP

In a spiking neural network [33,34], the message between neurons is encoded in spike trains, similar to the biological neural network. Spikes are signals discretized in time, which occur when the potential of a neuron reaches a threshold. The spike of one neuron influences the potential of other neurons connected through synapses. A synapse, as shown in Fig. 1(a), is directional. In the STDP model [31,32], the connection between two neurons evolves according to the relative timing between presynaptic and postsynaptic spikes: The connection is strengthened when presynaptic neuron spikes before the postsynaptic neuron within a finite time window, and the connection is weakened when presynaptic neuron spikes after the postsynaptic neuron. Spiking neural networks with the STDP learning rule are capable of various machine learning tasks, such as unsupervised learning of digit recognition [37,38].

Although all ANNs mimic the brain at some level, spiking neural networks with the STDP learning rule are more biologically plausible than others, e.g., sigmoid neurons [4,5]. In a neural network with sigmoid neurons, usually the message between neurons is a real number, each neuron is a differentiable function, and the connection between two neurons is characterized by a weight; then weights of connections and other parameters of the network are updated in the optimization of an objective function using methods such as gradient descent. In this paper, we present a key building block of quantum spiking neural network, i.e., a quantum gate that mimics the behavior of synapse in STDP.

III. MEMRISTIVE QUANTUM GATES

To find quantum gates with the memristive properties, we introduce a simplified picture of the memristor, which is different from actual memristive devices [30]. When we send the input current to memristor, the current is transmitted or reflected depending on the state of memristor, and the state of memristor evolves depending on the input current. If the input current is from A to B [see Fig. 1(b)], the resistance of memristor decreases. If the input current is from B to A, the resistance increases. We use one qubit to represent the current state: $|0\rangle_C$ and $|1\rangle_C$ denote currents from A to B and from B to A, respectively. We use another qubit to represent the resistance state: $|0\rangle_R$ and $|1\rangle_R$ denote transmission and reflection, respectively. In the extreme case, the resistance state can be completely flipped in one shot, then memristor is the transformation $|0\rangle_C \otimes |0\rangle_R \to |0\rangle_C \otimes |0\rangle_R$, $|0\rangle_C \otimes |1\rangle_R \to |1\rangle_C \otimes |0\rangle_R$, $|1\rangle_C \otimes |0\rangle_R \to |1\rangle_C \otimes |1\rangle_R$, and $|1\rangle_C \otimes |1\rangle_R \to |0\rangle_C \otimes |1\rangle_R$. The key point is that input states and output states of this transformation are both orthogonal. Therefore, it can be a unitary transformation, i.e., a quantum gate.

Now, we consider the general case that the resistance state is rotated by a finite angle of $\pi - 2\theta$ when it is not saturated. The corresponding unitary transformation reads

$$M_\theta = \begin{pmatrix} 1 & 0 & 0 & 0 \\ 0 & 0 & 0 & e^{i\theta} \\ 0 & \cos\theta & i\sin\theta & 0 \\ 0 & ie^{-i\theta}\sin\theta & e^{-i\theta}\cos\theta & 0 \end{pmatrix}, \tag{1}$$

where basis vectors are sorted as $|0\rangle_C \otimes |0\rangle_R$, $|0\rangle_C \otimes |1\rangle_R$, $|1\rangle_C \otimes |0\rangle_R$, and $|1\rangle_C \otimes |1\rangle_R$. When $\theta = 0$, M_θ can flip the resistance state in one shot as in the extreme case. When θ is finite, the gate transforms the input state $|0\rangle_C \otimes |1\rangle_R$ into $|1\rangle_C \otimes (\cos\theta|0\rangle_R + ie^{-i\theta}\sin\theta|1\rangle_R)$, i.e., the current is reflected, and the resistance state is rotated by a finite angle. It is similar for the input state $|1\rangle_C \otimes |0\rangle_R$. We can find that the influence of input current on the resistance state is minimized at $\theta = \frac{\pi}{2}$.

Many similar memristive gates can be constructed. For example, we can change the phases $e^{i\theta}$ and $e^{-i\theta}$, and the gate is still memristorlike. We choose the phases such that the gate M_θ can be used for encoding a quantum state and implementing universal quantum computing on the neural network, as we will show later.

In some scenarios, we want to use different qubits to represent the states of two terminals A and B. For example, we use two qubits A and B to represent voltages of two terminals. We can modify the memristive gate by taking $|0\rangle_C = |1\rangle_A \otimes |0\rangle_B$

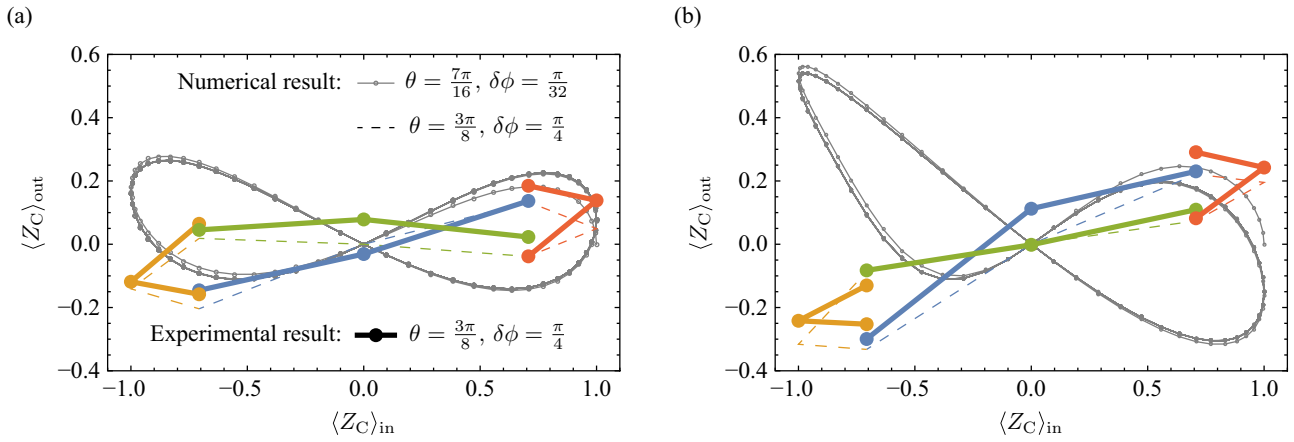

FIG. 2. Hysteresis loops of memristive gates. Here $\langle Z_C\rangle_{in}$ and $\langle Z_C\rangle_{out}$ represent the voltage and current, respectively. The phase $\eta = 1$ in (a) and $\eta = i$ in (b).

and $|1\rangle_C = |0\rangle_A \otimes |1\rangle_B$. Then, a three-qubit memristive gate is $\widetilde{M}_\theta = M_\theta \oplus \mathbb{1}_4$, where $\mathbb{1}_4$ is the four-dimensional identity matrix acting on the subspace of $|0\rangle_A \otimes |0\rangle_B \otimes |\mu\rangle_R$ and $|1\rangle_A \otimes |1\rangle_B \otimes |\mu\rangle_R$, i.e., the state of memristor does not change when two terminals have the same voltage. Qubits A and B can also be used to represent the spike timings of two neurons when the resistance qubit mimics the synapse. Memristive quantum gates for multistate current and resistance can be constructed in a similar way. In this paper, we focus on the two-qubit gate for simplicity.

IV. MEMRISTIVE BEHAVIOR

Let ρ_C and ρ_R be input states of the current qubit and resistance qubit, respectively. Then the output state after the memristive gate is $\rho_{out} = M_\theta \rho_C \otimes \rho_R M_\theta^\dagger$. We use I, X, Y, and Z to denote single-qubit Pauli operators. Considering mean values of Z, we have

$$\begin{aligned}\langle Z_C\rangle_{out} &= \mathrm{Tr}(Z \otimes I\rho_{out}) \\ &= \mathrm{Tr}(Z \otimes Z\rho_C \otimes \rho_R) = \langle Z_R\rangle_{in}\langle Z_C\rangle_{in}. \end{aligned} \quad (2)$$

Here, we have used $M_\theta^\dagger Z \otimes I M_\theta = Z \otimes Z$. We can find that Eq. (2) coincides with Ohm's law, i.e., $\langle Z_C\rangle_{in} = \mathrm{Tr}(Z\rho_C)$, $\langle Z_R\rangle_{in} = \mathrm{Tr}(Z\rho_R)$, and $\langle Z_C\rangle_{out} = \mathrm{Tr}(Z \otimes I\rho_{out})$ play the roles of voltage, conductance, and current, respectively.

To demonstrate the hysteretic behavior, we let the resistance qubit interact with a sequence of current qubits in input states $\rho_C^{(0)}, \rho_C^{(1)}, \ldots, \rho_C^{(t)}, \ldots$ one by one through memristive gates. Here, t is the label of time. Given any function of the voltage $\langle Z_C\rangle_{in}(t) = V(t) \in [-1, 1]$, the corresponding input states are $\rho_C^{(t)} = |\psi(t)\rangle\langle\psi(t)|$, where $|\psi(t)\rangle = \cos\frac{\phi(t)}{2}|0\rangle + \eta \sin\frac{\phi(t)}{2}|1\rangle$, $\phi(t) = \arccos(V(t))$, and $\eta = e^{i\varphi}$ can be any phase. We can prepare the state $|\psi(t)\rangle$ by applying single-qubit gates $R_y(\phi) = e^{-i\frac{\phi}{2}Y}$ and then $R_z(\varphi) = e^{-i\frac{\varphi}{2}Z}$ on the initial state $|0\rangle$.

Driven by current qubits, the resistance state evolves with t, which results in the hysteretic behavior. The $\langle Z_C\rangle_{out}$-versus-$\langle Z_C\rangle_{in}$ (i.e., current-versus-voltage) hysteresis loops are shown in Fig. 2, and the corresponding $\langle Z_R\rangle_{out}$-versus-$\langle Z_C\rangle_{in}$ curves are shown in Fig. 3. In these plots, we take $\phi(t) = \delta\phi t$ ($t = 0, 1, 2, \ldots$) and $\eta = 1, i$. In general, the shape of the hysteresis loop depends on the voltage form. For some voltage forms, a memristor behaves like a rectifier, i.e., current in the direction increasing the resistance is blocked. In our case, the shape of hysteresis loop also depends on the value of quantum phase η. In Fig. 2, the voltage form is the same $\langle Z_C\rangle_{in}(t) = \cos(\delta\phi t)$ for both values of η; however, the hysteresis loops have different shapes.

A. Numerical simulation

In the numerical simulation, the resistance qubit is initialized in the state $\rho_R^{(0)} = |+\rangle\langle+|$, where $|+\rangle = \frac{1}{\sqrt{2}}(|0\rangle + |1\rangle)$. With this initial state, we compute the output states of the first gate, $\rho_{out}^{(0)} = M_\theta \rho_C^{(0)} \otimes \rho_R^{(0)} M_\theta^\dagger$ and $\rho_R^{(1)} = \mathrm{Tr}_C(\rho_{out}^{(0)})$; with the output resistance state of the first gate, we compute the output states of the second gate, $\rho_{out}^{(1)} = M_\theta \rho_C^{(1)} \otimes \rho_R^{(1)} M_\theta^\dagger$ and $\rho_R^{(2)} = \mathrm{Tr}_C(\rho_{out}^{(1)})$, and so on. In this way, we can obtain output states of each gate. Then, at the time t, the voltage is $\langle Z_C\rangle_{in}(t) = \mathrm{Tr}(Z\rho_C^{(t)})$, the output current is $\langle Z_C\rangle_{out}(t) = \mathrm{Tr}(Z \otimes I\rho_{out}^{(t)})$, and the output conductance is $\langle Z_R\rangle_{out}(t) = \mathrm{Tr}(I \otimes Z\rho_{out}^{(t)})$.

In Figs. 2 and 3, small gray circles, respectively, represent the numerical data of $(\langle Z_C\rangle_{in}(t), \langle Z_C\rangle_{out}(t))$ and $(\langle Z_C\rangle_{in}(t), \langle Z_R\rangle_{out}(t))$ with $\theta = \frac{7\pi}{16}$ and $\delta\phi = \frac{\pi}{32}$, where $t = 0, 1, \ldots, \frac{20\pi}{\delta\phi} - 1$. Dashed lines represent the numerical data with $\theta = \frac{3\pi}{8}$ and $\delta\phi = \frac{\pi}{4}$. For dashed lines, the numerical simulations are implemented for $t = 0, 1, \ldots, \frac{20\pi}{\delta\phi} + 1$, however, only the last cycle (i.e., $t = \frac{20\pi}{\delta\phi} - 7, \frac{20\pi}{\delta\phi} - 6, \ldots, \frac{20\pi}{\delta\phi} + 1$) is plotted. The codes used to generate numerical results in this paper have been made openly available online [39].

B. Experiment

The superconducting quantum computer *ibmq_vigo* has five qubits. Two-qubit gates are available on nearest neighboring qubits (0,1), (1,2), (1,3), and (3,4). Only qubits 0,1,2,3 are used in our experiments: In experiments of the hysteretic behavior, LTP, LTD, and quantum state encoding, we always use the qubit 1 as the resistance qubit and qubits 0,2,3 as current qubits. In the calibration data from IBM Quantum Experience on 25 Feb 2020, single-qubit-gate error rates are from 0.03% to 0.07%, and two-qubit gate error rates are from 0.68% to

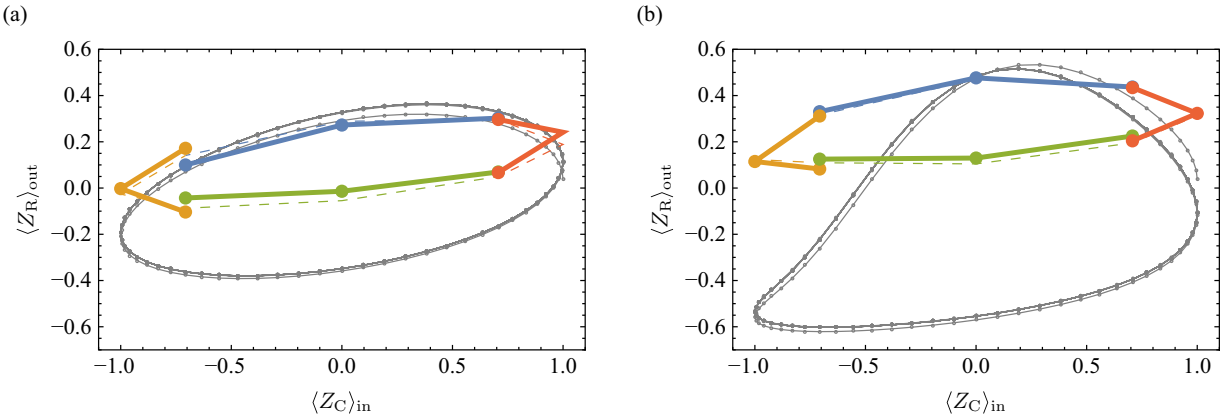

FIG. 3. Hysteresis loops of $(\langle Z_C\rangle_{in}(t), \langle Z_R\rangle_{out}(t))$. Here $\langle Z_C\rangle_{in}$ and $\langle Z_R\rangle_{out}$ represent the voltage and conductance, respectively. The phase $\eta = 1$ in (a) and $\eta = i$ in (b).

1.18%, depending on the qubits. We performed experiments on 25–27 Feb 2020. Each circuit runs for 8192 shots.

Because of the topology of qubit network on *ibmq_vigo*, we implement the memristive gates between the resistance qubit and at most three current qubits. To demonstrate a full cycle of each hysteresis loop, we divide the cycle into four segments, as shown in Figs. 2 and 3. In the experiment, we take $\theta = \frac{3\pi}{8}$ and $\delta\phi = \frac{\pi}{4}$ as the same as in numerical simulations of the dashed lines. For the segment started at $t = s$, we prepare the resistance qubit in the numerically-computed output state $\rho_R^{(s)}$, and then we let the resistance qubit interact with three current qubits prepared in states $\rho_C^{(s)}$, $\rho_C^{(s+1)}$, and $\rho_C^{(s+2)}$ one by one. The starting time of four segments are, respectively, $s = \frac{20\pi}{\delta\phi} - 7$, $\frac{20\pi}{\delta\phi} - 5$, $\frac{20\pi}{\delta\phi} - 3$, $\frac{20\pi}{\delta\phi} - 1$. Mean values $\langle Z_C\rangle_{out}(t)$ and $\langle Z_R\rangle_{out}(t)$ are measured in the experiment, and $(\langle Z_C\rangle_{in}(t), \langle Z_C\rangle_{out}(t))$ and $(\langle Z_C\rangle_{in}(t), \langle Z_R\rangle_{out}(t))$ are plotted as large circles in Figs. 2 and 3, respectively. If quantum gates are ideal, experimental data should be consistent with dashed lines. The difference is caused by the noise on *ibmq_vigo*. To minimize the impact of noise, we decompose the memristive gate into elementary gates as shown in Fig. 4(c).

Suppose we have enough qubits (or we can reuse the same current qubit and reinitialize it at each time t), we can directly implement a full cycle without dividing it into segments. Results of such a full-cycle experiment and the segmented-cycle experiment may have a discrepancy. Because the quantum computer is imperfect, each memristive gate causes some noise on the resistance qubit, making its state deviate from the one without noise (the numerical result). Such noise is ignored (compared to a full-cycle experiment) when we prepare the resistance qubit in the numerically-computed state at the beginning of each segment.

V. LONG-TERM PLASTICITY

In STDP, causal events increase the strength of a synapse, and acausal events decrease the strength, which are called LTP and LTD, respectively. LTP and LTD can be mimicked using the memristor [32]. In the memristive gate, the resistance state evolves driven by the current qubit. The output state of resistance qubit is $\mathcal{M}_{\theta,\rho_C}(\rho_R) = \mathrm{Tr}_C(\rho_{out})$, where Tr_C denotes the partial trace on the current qubit, and $\mathcal{M}_{\theta,\rho_C}$ is a completely positive map depending on θ and the input state ρ_C of current qubit. The steady state of this map is $\rho_s = \frac{1}{2}(I + \langle Z_C\rangle_{in} Z)$ (see Sec. V A). Therefore, after the interaction with a sequence of current qubits in the same input state, the conductance of memristor converges to $\langle Z_R\rangle_s = \langle Z_C\rangle_{in}$, i.e., the classical information of current qubit is encoded into the resistance qubit.

A. Steady state in long-term plasticity

We express the map on a qubit using the Pauli transfer matrix representation. The state of a qubit can be written as a linear combination of Pauli operators: The input state of the current qubit is $\rho_C = \frac{1}{2}(I + \rho_C^X X + \rho_C^Y Y + \rho_C^Z Z)$, the input state of the resistance qubit is $\rho_R = \frac{1}{2}(I + \rho_R^X X + \rho_R^Y Y + \rho_R^Z Z)$, the output state of the resistance qubit is $\rho_{R,out} = \mathcal{M}_{\theta,\rho_C}(\rho_R) = \frac{1}{2}(I + \rho_{R,out}^X X + \rho_{R,out}^Y Y + \rho_{R,out}^Z Z)$. We can find that each qubit state corresponds to a vector of which elements are coefficients of Pauli operators. Accordingly, we can express a linear map on the state as a matrix acting on the corresponding vector. The Pauli transfer matrix of the memristive-gate map $\mathcal{M}_{\theta,\rho_C}$ is

$$M_{\theta,\rho_C} = \begin{pmatrix} 1 & 0 \\ k & E \end{pmatrix}, \tag{3}$$

where

$$k = \rho_C^Z \begin{pmatrix} \cos\theta \sin^2\theta \\ \cos^2\theta \sin\theta \\ \cos^2\theta \end{pmatrix} \tag{4}$$

and

$$E = \begin{pmatrix} \rho_C^X \cos\theta - \rho_C^Y \sin^3\theta & -\rho_C^X \cos^2\theta \sin\theta & -\cos\theta \sin^2\theta \\ \rho_C^Y \cos^3\theta & \rho_C^X \cos\theta \sin^2\theta - \rho_C^Y \sin\theta & -\cos^2\theta \sin\theta \\ -\rho_C^Y \cos\theta \sin\theta & \rho_C^X \cos\theta \sin\theta & \sin^2\theta \end{pmatrix}. \tag{5}$$

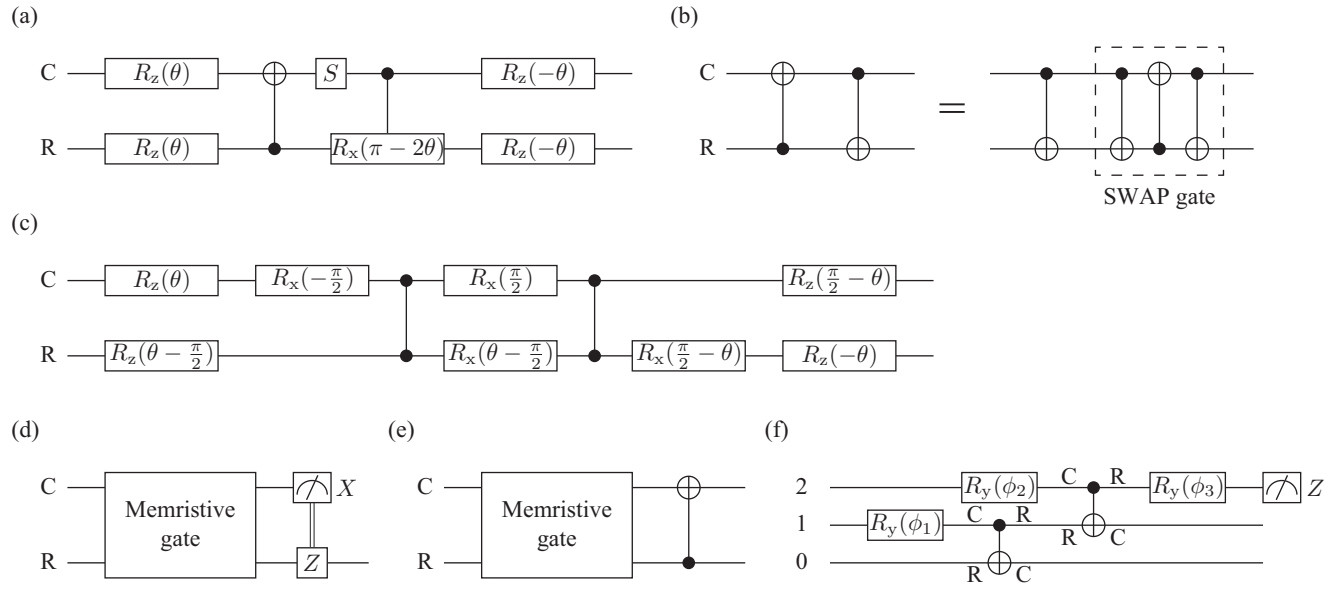

FIG. 4. (a) The circuit in Fig. 1(c) displayed using rotation gates with angles, $R_x(\phi) = e^{-i\frac{\phi}{2}X}$, $R_y(\phi) = e^{-i\frac{\phi}{2}Y}$, and $R_z(\phi) = e^{-i\frac{\phi}{2}Z}$. (b) Circuit of the memristive gate M_0. (c) Circuit of the memristive gate M_θ optimized for the implementation on *ibmq_vigo*. (d) Circuit of the modified memristive gate with a measurement on the current qubit and a feedback gate on the resistance qubit. (e) Circuit of the modified memristive gate with an additional controlled-NOT gate, which is used in the experiment on *ibmq_vigo*. (f) Circuit of the quantum state classification experiment on *ibmq_vigo*.

Then, we have

$$\begin{pmatrix} \rho^X_{\mathrm{R,out}} \\ \rho^Y_{\mathrm{R,out}} \\ \rho^Z_{\mathrm{R,out}} \end{pmatrix} = E \begin{pmatrix} \rho^X_{\mathrm{R}} \\ \rho^Y_{\mathrm{R}} \\ \rho^Z_{\mathrm{R}} \end{pmatrix} + k. \tag{6}$$

The steady state of the map $\mathcal{M}_{\theta,\rho_C}$ is the solution of the equation $\rho_s = \mathcal{M}_{\theta,\rho_C}(\rho_s)$. Express the steady state in the form $\rho_s = \frac{1}{2}(I + \rho^X_s X + \rho^Y_s Y + \rho^Z_s Z)$, the equation becomes

$$\begin{pmatrix} \rho^X_{\mathrm{s}} \\ \rho^Y_{\mathrm{s}} \\ \rho^Z_{\mathrm{s}} \end{pmatrix} = E \begin{pmatrix} \rho^X_{\mathrm{s}} \\ \rho^Y_{\mathrm{s}} \\ \rho^Z_{\mathrm{s}} \end{pmatrix} + k, \tag{7}$$

and its solution is

$$\begin{pmatrix} \rho^X_{\mathrm{s}} \\ \rho^Y_{\mathrm{s}} \\ \rho^Z_{\mathrm{s}} \end{pmatrix} = \begin{pmatrix} 0 \\ 0 \\ \rho^Z_{\mathrm{C}} \end{pmatrix}. \tag{8}$$

We remark that $\rho^Z_{\mathrm{C}} = \mathrm{Tr}(Z\rho_{\mathrm{C}}) = \langle Z_{\mathrm{C}}\rangle_{\mathrm{in}}$.

B. LTP and LTD

To demonstrate LTP and LTD phenomena mimicked using memristive gates, we take $\rho_{\mathrm{C}} = |0\rangle\langle 0|$ and $\rho_{\mathrm{C}} = |1\rangle\langle 1|$ to represent causal events in LTP and acausal events in LTD, respectively. We also take $\rho_{\mathrm{C}} = |+\rangle\langle +|$ to represent stochastic events (SE) without a definite casual order, where $|\pm\rangle = \frac{1}{\sqrt{2}}(|0\rangle \pm |1\rangle)$. Results of numerical simulation and experiment are shown in Fig. 5(a). These results are obtained with two-qubit memristive gates. We can obtain similar results with three-qubit memristive gates by using qubits A and B to represent spike timings of two neurons, respectively.

In the numerical simulation, we let the resistance qubit interact with a sequence of current qubits in the input states $\rho^{(0)}_{\mathrm{C}}, \rho^{(1)}_{\mathrm{C}}, \ldots, \rho^{(t)}_{\mathrm{C}}, \ldots$ one by one through memristive gates, as the same as in hysteresis-loop simulation. We take $\rho^{(t)}_{\mathrm{C}} = |1\rangle\langle 1|$ when $t = 0, 1, \ldots, 99$, $\rho^{(t)}_{\mathrm{C}} = |0\rangle\langle 0|$ when $t = 100, 101, \ldots, 199$, $\rho^{(t)}_{\mathrm{C}} = |1\rangle\langle 1|$ again when $t = 200, 201, \ldots, 299$, and $\rho^{(t)}_{\mathrm{C}} = |+\rangle\langle +|$ when $t = 300, 301, \ldots, 399$. The resistance qubit is initialized in the state $\rho^{(0)}_{\mathrm{R}} = |+\rangle\langle +|$. With this initial state, we compute output states of the resistance qubit, i.e., $\rho^{(t+1)}_{\mathrm{R}} = \mathcal{M}_{\theta,\rho^{(t)}_{\mathrm{C}}}(\rho^{(t)}_{\mathrm{R}})$, where $\theta = \frac{7\pi}{16}$. Then, $\langle Z_{\mathrm{R}}\rangle_{\mathrm{out}}(t) = \mathrm{Tr}(Z\rho^{(t)}_{\mathrm{R}})$ is computed and plotted as the thin curve in Fig. 5(a).

Four experiments of LTP and LTD are implemented on *ibmq_vigo*, corresponding to four thick curves (with circles) in Fig. 5(a). From left to right in the plot, the initial state of the resistance qubit is $|+\rangle$, $|1\rangle$, $|0\rangle$, and $|1\rangle$ in the four experiments, respectively, and the initial state of currents qubits is, respectively, $|1\rangle$, $|0\rangle$, $|1\rangle$, and $|+\rangle$. We let the resistance qubit interact with three current qubits one by one through the memristive gate. We take $\theta = \frac{\pi}{4}$ in the memristive gate, and the gate is decomposed into elementary gates as shown in Fig. 4(c). After each memristive gate, $\langle Z_{\mathrm{R}}\rangle_{\mathrm{out}}$ is measured.

VI. ENCODING QUANTUM STATES

Memristive gates can encode quantum information into the resistance qubit. In LTP and LTD processes, only the classical information is encoded because the phase information is not preserved. The current qubit is flipped or not flipped depending on the resistance state. Therefore two qubits are correlated in the Z direction in the output state, which damages the phase information. To restore the phase, we can measure the output

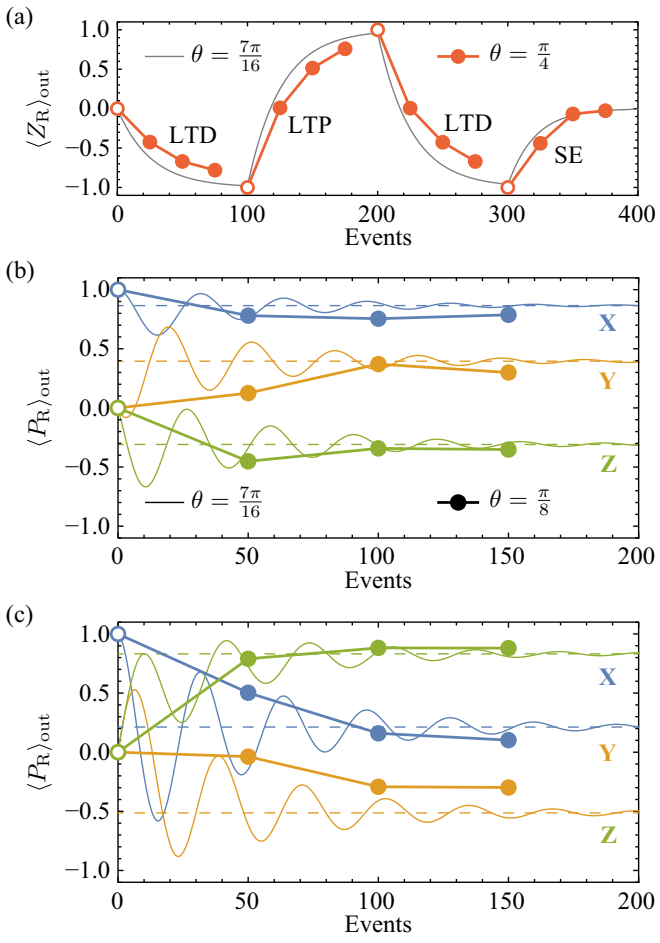

FIG. 5. (a) Classical and (b),(c) quantum long-term plasticity based on memristive gates. Thin solid curves represent numerical results, and filled circles represent experimental results. Empty circles denote initial values in the experiments. In (b) and (c), we take the same values of the parameter θ. Dashed horizontal lines denote values in the input state of current qubits, i.e., the steady state. $P = X, Y, Z$ are Pauli operators. The quantum state is successfully encoded when three $\langle P_R\rangle_{out}$ converge to dashed lines.

current qubit in the X basis and adjust the phase of resistance qubit, see Fig. 4(d): The identity gate I or phase gate Z on the resistance qubit is performed if the measurement outcome is $|+\rangle$ or $|-\rangle$, respectively. Accordingly, the map on resistance qubit reads $\mathcal{M}'_{\theta,\rho_C}(\rho_R) = \mathrm{Tr}_C(K_+\rho_{out}K_+) + \mathrm{Tr}_C(K_-\rho_{out}K_-)$, where $K_\eta = |\eta\rangle\langle\eta| \otimes Z^{\frac{1}{2}-\eta\frac{1}{2}}$. The steady state of this map is $\rho'_s = \rho_C$ (see Sec. VI A). Therefore, after the interaction with a sequence of current qubits in the same input state, the resistance state converges to ρ_C, i.e., quantum information is encoded.

A. Steady state in the quantum state encoding

In the Pauli transfer matrix representation, the matrix of the memristive-gate map $\mathcal{M}'_{\theta,\rho_C}$ is

$$M'_{\theta,\rho_C} = \begin{pmatrix} 1 & 0 \\ k' & E' \end{pmatrix}, \tag{9}$$

where

$$k' = \cos^2\theta \begin{pmatrix} \rho_C^X \\ \rho_C^Y \\ \rho_C^Z \end{pmatrix} \tag{10}$$

and

$$E' = \begin{pmatrix} \sin^2\theta & -\rho_C^Z\cos\theta\sin\theta & \rho_C^Y\cos\theta\sin\theta \\ \rho_C^Z\cos\theta\sin\theta & \sin^2\theta & -\rho_C^X\cos\theta\sin\theta \\ -\rho_C^Y\cos\theta\sin\theta & \rho_C^X\cos\theta\sin\theta & \sin^2\theta \end{pmatrix}. \tag{11}$$

Let $\rho'_s = \frac{1}{2}(I + \rho_s'^X X + \rho_s'^Y Y + \rho_s'^Z Z)$ be the steady state of $\mathcal{M}'_{\theta,\rho_C}$. By solving the steady state equation (see Sec. V A), we can find that

$$\begin{pmatrix} \rho_s'^X \\ \rho_s'^Y \\ \rho_s'^Z \end{pmatrix} = \begin{pmatrix} \rho_C^X \\ \rho_C^Y \\ \rho_C^Z \end{pmatrix}. \tag{12}$$

Therefore, $\rho'_s = \rho_C$.

B. Demonstration of the quantum state encoding

We take two input states to demonstrate the quantum state encoding, and results are shown in Figs. 5(b) and 5(c). The resistance qubit is initialized in the state $\rho_R^{(0)} = |+\rangle\langle+|$. We let the resistance qubit interact with a sequence of current qubits in the input states $\rho_C^{(0)}, \rho_C^{(1)}, \ldots, \rho_C^{(t)}, \ldots$ one by one through modified memristive gates. In both numerical simulation and experiment, we take $\rho_C^{(t)} = |\psi\rangle\langle\psi|$ for all t, where $|\psi\rangle = e^{-i\frac{7\pi}{22}Z}e^{-i\frac{3\pi}{10}X}|0\rangle$ in (b) and $|\psi\rangle = e^{-i\frac{\pi}{16}Z}e^{-i\frac{3\pi}{32}X}|0\rangle$ in (c). The circuit of modified memristive gate (encoding gate) is shown in Fig. 4(d). Because we are only interested in the state of the resistance qubit, the modified memristive gate can also be realized using the circuit shown in Fig. 4(e). The additional controlled-NOT gate in Fig. 4(e) is equivalent to a phase gate on the resistance qubit depending on the phase state of the current qubit.

In the numerical simulation, we compute the output state of the resistance qubit at each time t, i.e., $\rho_R^{(t+1)} = \mathcal{M}'_{\theta,\rho_C^{(t)}}(\rho_R^{(t)})$, where $\theta = \frac{7\pi}{16}$. Then, the mean values of three Pauli operators $\langle P_R\rangle_{out}(t) = \mathrm{Tr}(P\rho_R^{(t)})$ are computed and plotted as thin solid curves in Figs. 5(b) and 5(c), where $P = X, Y, Z$. In the two experiments implemented on *ibmq_vigo*, we take $\theta = \frac{\pi}{8}$, and the modified memristive gate is realized using the circuit in Fig. 4(e), in which the memristive gate is decomposed into elementary gates as shown in Fig. 4(c). The mean values of Pauli operators $\langle P_R\rangle_{out}$ are measured after each modified memristive gate and plotted as thick curves (with circles) in Figs. 5(b) and 5(c).

In the two experiments, the encoding fidelity, respectively, reaches 97.672% and 97.638% after three memristive gates. We can express states of the current qubit and resistance qubit as $\rho_C^{(t)} = \frac{1}{2}(I + \rho_C^X X + \rho_C^Y Y + \rho_C^Z Z)$ and $\rho_R^{(t)} = \frac{1}{2}(I + \rho_R^X X + \rho_R^Y Y + \rho_R^Z Z)$, respectively. Here, $\rho_C^P = \mathrm{Tr}(P\rho_C^{(t)})$ and $\rho_R^P = \mathrm{Tr}(P\rho_R^{(t)})$. Therefore, when $\mathrm{Tr}(P\rho_C^{(t)}) = \mathrm{Tr}(P\rho_R^{(t)})$ for all P, two states are the same. In Figs. 5(b) and 5(c), the dashed horizontal lines represent $\mathrm{Tr}(P\rho_C^{(t)})$. Because

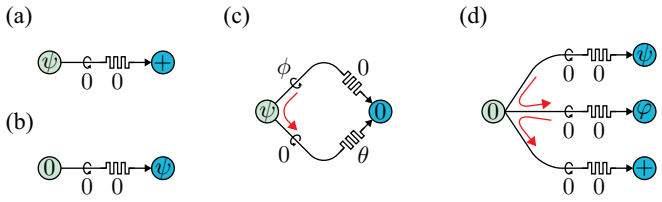

FIG. 6. Universal quantum computing operations on the neural network, including (a) write operation, (b) read operation, (c) single-qubit gate, and (d) two-qubit gate. Red arrows denote the time sequence.

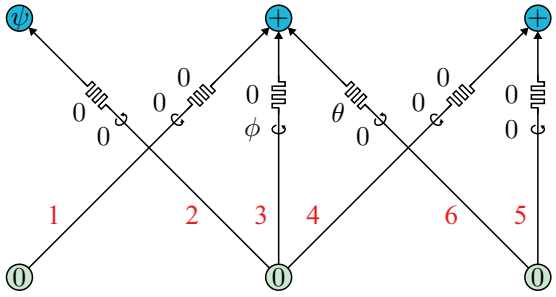

FIG. 7. Single-qubit gate. Red numbers denote the time sequence.

$\rho_C^{(t)}$ is a pure state, the fidelity is $F = \sqrt{\mathrm{Tr}(\rho_C^{(t)}\rho_R^{(t)})} = \sqrt{(1+\rho_C^X\rho_R^X+\rho_C^Y\rho_R^Y+\rho_C^Z\rho_R^Z)/2}$.

VII. ARTIFICIAL NEURAL NETWORK

The neural network in Fig. 1(d) has three layers. The input layer and hidden layer are formed by M current qubits and N resistance qubits, respectively. Each connection between two quantum layers has three labels (i, a, b) and two parameters (ϕ_i, θ_i): The ith connection is a composite gate $M_{\theta_i}e^{-i\frac{\phi_i}{2}Y}\otimes I$ on the ath current qubit and bth resistance qubit. Here, the Y-axis rotation is on the current qubit. We remark that these connections are time ordered according to i because quantum gates are noncommutative. The output layer is formed by N classical bits. Each resistance qubit and the corresponding classical bit has a connection with only one parameter ϕ_j: After a Y-axis rotation $e^{-i\frac{\phi_j}{2}Y}$, the resistance qubit is measured in the Z basis, and outcome is the classical bit.

VIII. UNIVERSAL QUANTUM COMPUTING

To implement universal quantum computing on the memristive ANN, we initialize input (current) and hidden-layer (resistance) qubits in states $|0\rangle$ and $|+\rangle$, respectively. We can think of that resistance qubits form the register of quantum data, and current qubits conduct the computing. (i) A current qubit can write/read the quantum state of a resistance qubit by taking $\phi = \theta = 0$, as shown in Fig. 6(a), corresponding to transformations $M_0|\psi\rangle\otimes|+\rangle = |+\rangle\otimes|\psi\rangle$ and $M_0|0\rangle\otimes|\psi\rangle = |\psi\rangle\otimes|0\rangle$, respectively. (ii) To perform a single-qubit gate, we let a current qubit carry the qubit state $|\psi\rangle$ and prepare a resistance qubit in the state $|0\rangle$ by using write/read operations. Then, by visiting the resistance qubit twice with parameters shown in Fig. 6(b), we obtain the transform $M_\theta M_0 e^{-i\frac{\phi}{2}Y}\otimes I|\psi\rangle\otimes|0\rangle = I\otimes e^{-i\frac{\theta}{2}Z}e^{-i\frac{\phi}{2}Y}|0\rangle\otimes|\psi\rangle$, which is a universal single-qubit gate. (iii) To perform a two-qubit gate on two resistance qubits, we use a current qubit to read the state of the first qubit ψ and let it interact with the second qubit φ [see Fig. 6(c)]. The output current state is written into the third resistance qubit. In this way, a controlled-NOT gate Λ_X is performed. The corresponding transformation on three resistance qubits is $|\Psi\rangle_{1,2}\otimes|+\rangle_3\to|0\rangle_1\otimes\Lambda_X|\Psi\rangle_{2,3}$, where $|\Psi\rangle$ is the input two-qubit state, and the second qubit is the control qubit in Λ_X. To understand the controlled-NOT gate, we only need to note that the memristive gate with $\theta = 0$, i.e., M_0, is equivalent to a controlled-NOT gate followed by a swap gate, as shown in Fig. 4(b). The universal single-qubit gate and controlled-NOT gate form a universal gate set [9].

The single-qubit gate can be implemented under the restriction that each current qubit can only visit a resistance qubit at most once. As shown in Fig. 7, connection-1 prepares the second resistance qubit (from left to right) in the state $|0\rangle$, connection-2 reads the state of the first resistance qubit $|\psi\rangle$ into the second current qubit, connection-3 corresponds to the first visit in Fig. 6(c), connection-4 writes the output state of second current qubit into the third resistance qubit, connection-5 reads the state of the third resistance qubit into the third current qubit, and connection-6 corresponds to the second visit in Fig. 6(c).

The overhead cost of universal quantum computing on the memristive ANN is polynomial. Each controlled-NOT gate consumes one current qubit and one resistance qubit. Under the one-visit restriction, each single-qubit gate consumes three current qubits and two resistance qubits. Therefore, the overhead factor is a constant.

IX. QUANTUM STATE CLASSIFICATION

Now, we use the memristive neural network for quantum state classification [22–24,35]. Input qubits are prepared in one of the quantum states to be classified $|\Phi_k\rangle$. Hidden-layer qubits are initialized in the state $|+\rangle$. The input layer and hidden layer are fully connected, and connections are sorted as follows: The first input qubit interacts with from the first to the Nth hidden-layer qubits one by one; then, the second input qubit interacts with from the first to the Nth hidden-layer qubits one by one; and so on. In other words, the ath input qubit and the bth hidden-layer qubit are coupled by the ith Y-axis rotation and memristive gate, where $i = N(a-1)+b$.

The probability distribution of output classical bits $\boldsymbol{\mu}$ depends on the input state $|\Phi_k\rangle$. Here, $\boldsymbol{\mu} = (\mu_1, \mu_2, \ldots, \mu_N)$ is a binary vector, μ_j is the value of the jth output bit, i.e., the measurement outcome of the jth hidden-layer qubit. The probability of $\boldsymbol{\mu}$ given the input state $|\Phi_k\rangle$ is $p_{\boldsymbol{\phi},\boldsymbol{\theta}}(\boldsymbol{\mu}|\Phi_k)$, where $\boldsymbol{\phi} = (\phi_1, \phi_2, \ldots, \phi_{(M+1)N})$ and $\boldsymbol{\theta} = (\theta_1, \theta_2, \ldots, \theta_{MN})$ are parameters of the neural network, and ϕ_{MN+j} is the parameter of the Y-axis rotation on the jth hidden-layer qubit before the measurement. We find the optimal parameters by maximizing $\overline{D} = \sum_{k\neq k'} D(p_{\boldsymbol{\phi},\boldsymbol{\theta}}(\bullet|\Phi_k), p_{\boldsymbol{\phi},\boldsymbol{\theta}}(\bullet|\Phi_{k'}))$. Here,

$$D(p_{\boldsymbol{\phi},\boldsymbol{\theta}}(\bullet|\Phi_k), p_{\boldsymbol{\phi},\boldsymbol{\theta}}(\bullet|\Phi_{k'})) = \frac{1}{2}\sum_{\boldsymbol{\mu}}|p_{\boldsymbol{\phi},\boldsymbol{\theta}}(\boldsymbol{\mu}|\Phi_k) - p_{\boldsymbol{\phi},\boldsymbol{\theta}}(\boldsymbol{\mu}|\Phi_{k'})| \quad (13)$$

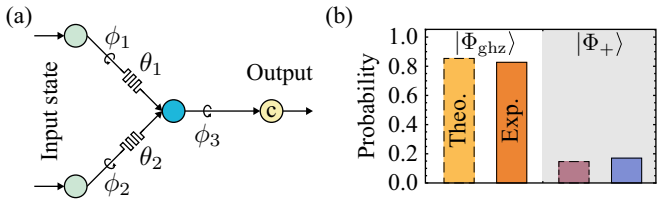

FIG. 8. (a) Neural network for the classification of two-qubit states. (b) Probability of the output bit 0 given optimal parameters. Dashed and solid boxes represent the theoretical and experimental results, respectively.

is the trace distance between two distributions [9], which characterizes how well two states can be distinguished according to the output $\boldsymbol{\mu}$.

Two examples are implemented. First, we use a network with two neurons in each layer, i.e., $M = N = 2$ to classify four Bell states. Because Bell states are orthogonal, they are completely distinguishable, which can be achieved by the neural network. Second, we use a network with $M = N = 5$ to classify two five-qubit ground states of the quantum Ising model in ferromagnetic and paramagnetic phases [40], i.e., the Greenberger-Horne-Zeilinger state $|\Phi_{\rm ghz}\rangle = \frac{1}{\sqrt{2}}(|0\rangle^{\otimes M} + |1\rangle^{\otimes M})$ and the product state $|\Phi_+\rangle = |+\rangle^{\otimes M}$. These two states are not orthogonal. We find that the maximum distance given by neural network can reach the quantum upper bound, i.e., the trace distance between two quantum states [9]. If we turn off parameters $\boldsymbol{\phi}$ by setting all ϕ to zero, only memristive gates are used in the classification. In this case, the distance can reach 0.94792, which is lower than the upper bound 0.96824 but is still above the classical value 0.9375, i.e., the distance given by a direct measurement in the Z basis on each qubit. For the experimental implementation, we use the network shown in Fig. 8(a) to classify two-qubit ground states. In the numerical simulation, the distance can reach the theoretical upper bound 0.70711, which is reduced to 0.65673 (but still higher than the classical value 0.5) in the experiment using optimal parameters. The corresponding distributions are shown in Fig. 8(b).

A. Numerical simulation of Bell-state classification

To distinguish four Bell states

$$|\Phi_1\rangle = \frac{1}{\sqrt{2}}(|0\rangle \otimes |0\rangle + |1\rangle \otimes |1\rangle), \tag{14}$$

$$|\Phi_2\rangle = \frac{1}{\sqrt{2}}(|0\rangle \otimes |0\rangle - |1\rangle \otimes |1\rangle), \tag{15}$$

$$|\Phi_3\rangle = \frac{1}{\sqrt{2}}(|0\rangle \otimes |1\rangle + |1\rangle \otimes |0\rangle), \tag{16}$$

$$|\Phi_4\rangle = \frac{1}{\sqrt{2}}(|0\rangle \otimes |1\rangle - |1\rangle \otimes |0\rangle), \tag{17}$$

we take $M = N = 2$, i.e., each layer has two qubits or classical bits. We find optimal parameters $\boldsymbol{\phi}$ and $\boldsymbol{\theta}$ by maximizing the distance function

$$\overline{D}(\boldsymbol{\phi}, \boldsymbol{\theta}) = \sum_{k=1}^{3} \sum_{k'=k+1}^{4} D(p_{\boldsymbol{\phi},\boldsymbol{\theta}}(\bullet|\Phi_k), p_{\boldsymbol{\phi},\boldsymbol{\theta}}(\bullet|\Phi_{k'})). \tag{18}$$

The value of the average distance $\overline{D}/6$ is plotted in Fig. 9(a), which reaches one at the end of the optimization. The distance D is never larger than 1, and $D = 1$ means that two states are fully distinguishable with the successful probability one. The optimal parameters are $\boldsymbol{\phi} = (0, -0.31973, 0, 0, -1.5708, 0)$ and $\boldsymbol{\theta} = (0, -1.3065, 0, 0)$. We note that $\frac{\pi}{2} \simeq 1.5708$, and changing values of ϕ_2 and θ_2 does not reduce the distance.

B. Numerical simulation of ground-state classification

The two ground states $|\Phi_{\rm ghz}\rangle$ and $|\Phi_+\rangle$ are not orthogonal. Therefore, they are not fully distinguishable. The trace distance between the two quantum states is

$$\begin{aligned} D(|\Phi_{\rm ghz}\rangle, |\Phi_+\rangle) &= \sqrt{1 - |\langle\Phi_+|\Phi_{\rm ghz}\rangle|^2} \\ &= \sqrt{1 - \frac{1}{2^{M-1}}}, \end{aligned} \tag{19}$$

where M is the number of qubits in the ground states. For any measurement setup, the distance between measurement-outcome distributions of two quantum states is never larger than $D(|\Phi_{\rm ghz}\rangle, |\Phi_+\rangle)$. Therefore, $D(p_{\boldsymbol{\phi},\boldsymbol{\theta}}(\bullet|\Phi_{\rm ghz}), p_{\boldsymbol{\phi},\boldsymbol{\theta}}(\bullet|\Phi_+)) \leqslant D(|\Phi_{\rm ghz}\rangle, |\Phi_+\rangle)$.

If two ground states are directly measured in the Z basis, the measurement-outcome distributions are $q(\boldsymbol{\mu}|\Phi_{\rm ghz}) = \frac{\delta_{\boldsymbol{\mu},\mathbf{0}} + \delta_{\boldsymbol{\mu},\mathbf{1}}}{2}$ and $q(\boldsymbol{\mu}|\Phi_+) = \frac{1}{2^M}$, where $\mathbf{0} = (0, 0, \ldots, 0)$ and $\mathbf{1} = (1, 1, \ldots, 1)$. The distance between the two distributions is

$$D(q(\bullet|\Phi_{\rm ghz}), q(\bullet|\Phi_+)) = 1 - \frac{1}{2^{M-1}}. \tag{20}$$

To distinguish two ground states of five qubits, we take $M = N = 5$, i.e., each layer has five qubits or classical bits. We find optimal parameters $\boldsymbol{\phi}$ and $\boldsymbol{\theta}$ by maximizing the distance function

$$\overline{D}(\boldsymbol{\phi}, \boldsymbol{\theta}) = D(p_{\boldsymbol{\phi},\boldsymbol{\theta}}(\bullet|\Phi_{\rm ghz}), p_{\boldsymbol{\phi},\boldsymbol{\theta}}(\bullet|\Phi_+)). \tag{21}$$

The result is plotted in Fig. 9(b), and $\overline{D}$ reaches the quantum upper bound $D(|\Phi_{\rm ghz}\rangle, |\Phi_+\rangle) \simeq 0.96824$ at the end of the optimization.

If we turn off parameters $\boldsymbol{\phi}$ by setting $\phi_i = 0$ for all $i = 1, 2, \ldots, (M+1)N$, we find the optimal $\boldsymbol{\theta}$ by maximizing the distance function

$$\overline{D}(\boldsymbol{\theta}) = D(p_{\mathbf{0},\boldsymbol{\theta}}(\bullet|\Phi_{\rm ghz}), p_{\mathbf{0},\boldsymbol{\theta}}(\bullet|\Phi_+)). \tag{22}$$

Here, $\mathbf{0}$ is the $(M+1)N$-dimensional zero vector. The result is plotted in Fig. 9(c), and $\overline{D}$ reaches 0.94792 at the end of the optimization, which is lower than $D(|\Phi_{\rm ghz}\rangle, |\Phi_+\rangle)$ but above $D(q(\bullet|\Phi_{\rm ghz}), q(\bullet|\Phi_+)) = 0.9375$.

C. Experiment of ground-state classification

In the experiment, we use a three-qubit neural network shown in Fig. 8(a), i.e., $M = 2$ and $N = 1$, to distinguish

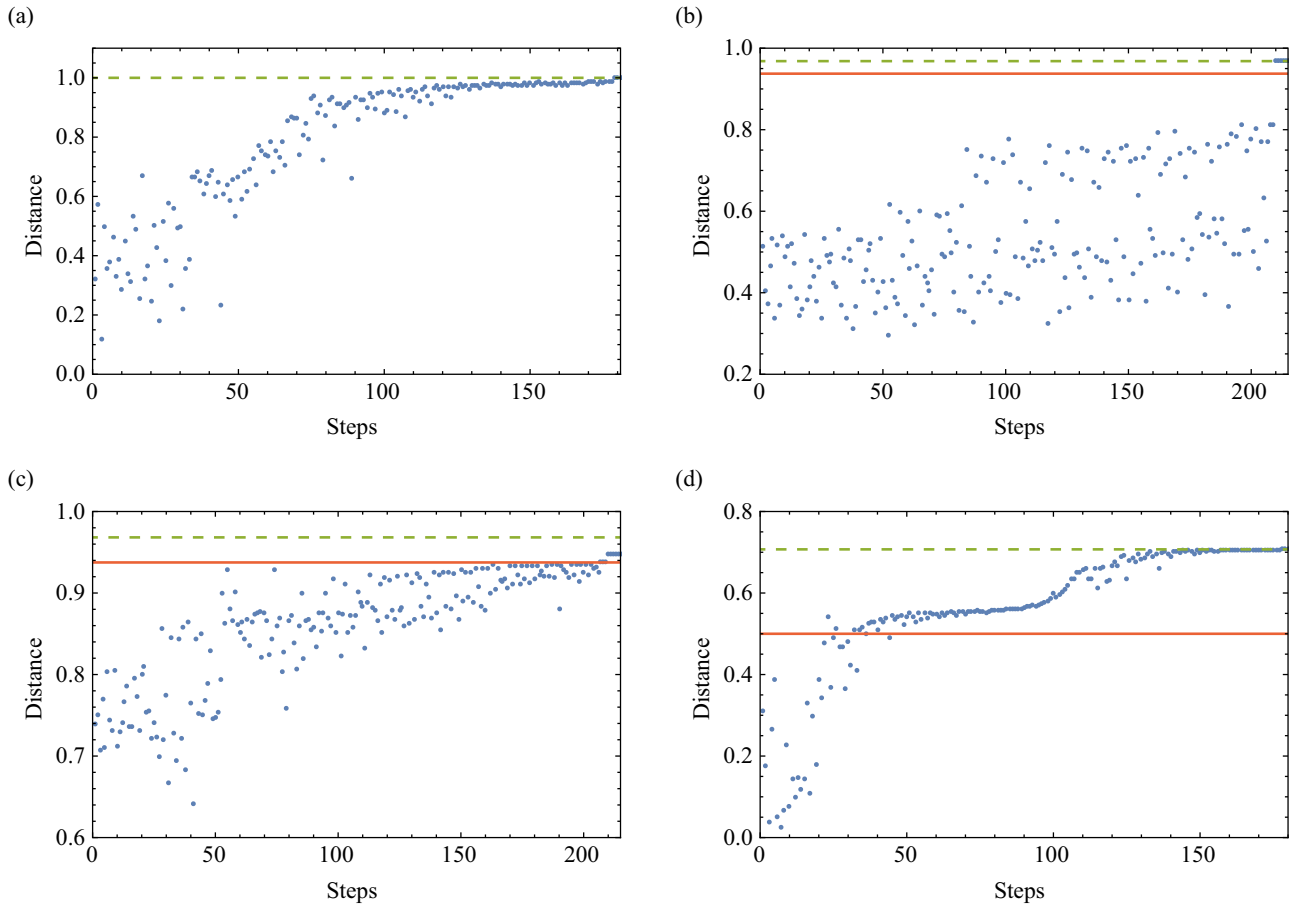

FIG. 9. Values of the distance in the optimisation computing for the classification of (a) Bell states, (b) ten-qubit Ising-model states with all parameters, (c) ten-qubit Ising-model states with reduced parameters, and (d) three-qubit Ising-model states. Blue dots denote the distance returned in each step. Dashed lines denote the quantum upper bound of the distance. Solid lines denote classical values, i.e., $D(q(\bullet|\Phi_{\rm ghz}), q(\bullet|\Phi_+))$.

two-qubit ground states. We find optimal parameters $\boldsymbol{\phi}$ and $\boldsymbol{\theta}$ by maximizing the distance function $\overline{D}(\boldsymbol{\phi}, \boldsymbol{\theta})$ [Eq. (21)], and the result is plotted in Fig. 9(d). The distance $\overline{D}$ reaches the quantum upper bound $D(|\Phi_{\rm ghz}\rangle, |\Phi_+\rangle) \simeq 0.70711$ at the end of the optimization. The optimal parameters are $\boldsymbol{\phi} = (1.5708, 1.5708, -0.78540)$ and $\boldsymbol{\theta} = (0, 0)$. We note that $\frac{\pi}{2} \simeq 1.5708$ and $\frac{\pi}{4} \simeq 0.78540$. These parameters are used in the experiment.

To implement the three-qubit neural network on *ibmq_vigo*, we optimize the circuit, i.e., minimize the number of two-qubit gates, as follows. We can find that only memristive gates M_θ with $\theta = 0$ are used according to optimal parameters. Each gate M_0 can be realized using two controlled-NOT gates, as shown in Fig. 4(b), which is equivalent to a controlled-NOT gate followed by a SWAP gate. Therefore, we can implement the neural network with optimal parameters as shown in Fig. 4(f): At the beginning, qubit-0 represents the resistance qubit (i.e., hidden-layer qubit), qubit-1 and qubit-2 represent current qubits (i.e., input qubits); to perform the first memristive gate, instead of physically performing the SWAP gate, the roles of qubit-0 and qubit-1 are exchanged after the first controlled-NOT gate, i.e., now qubit-1 represents the resistance qubit, and qubit-0 represents a current qubit; It is similar for the second memristive gate. The distributions of measurement outcomes obtained in the experiment are shown in Fig. 8(b). The distance between distributions of two ground states is 0.65673, which is lower than the theoretical value $D(|\Phi_{\rm ghz}\rangle, |\Phi_+\rangle) \simeq 0.70711$ but above $D(q(\bullet|\Phi_{\rm ghz}), q(\bullet|\Phi_+)) = 0.5$.

X. DISCUSSION

We have demonstrated that memristive quantum gates can mimic memristors and synapses, which are essential building blocks of spike-based neuromorphic computing. These gates are unitary transformations that are feasible in many physical systems [9]. Memristive gates are fully quantum compared with the memristance involving the weak measurement and dissipation in quantum systems [41–46]. The experiments are implemented using universal gates on a circuit-based quantum computer *ibmq_vigo*. By engineering the interaction between qubits, it is also possible to realize a memristive gate directly in the time evolution. Synapses based on memristive

gates can encode the quantum state in a way similar to the long-term plasticity, therefore, are capable of processing quantum information. We have proposed a nonspiking ANN built on memristive gates. The question that we have not discussed in this work is how to combine memristive gates with spiking neurons in the quantum regime [47] to construct a quantum spiking neural network, which is worth future exploration.

ACKNOWLEDGMENTS

We acknowledge the use of simulation toolkit QuESTlink and IBM Quantum services for this work. This work is supported by National Natural Science Foundation of China (Grants No. 11875050 and No. 12088101) and NSAF (Grant No. U1930403). Y.L. thanks Tyson Jones for help on using QuESTlink.

[1] C. Mead, Neuromorphic electronic systems, Proc. IEEE **78**, 1629 (1990).

[2] C. D. Schuman, T. E. Potok, R. M. Patton, J. D. Birdwell, M. E. Dean, G. S. Rose, J. S. Plank, A survey of neuromorphic computing and neural networks in hardware, arXiv:1705.06963.

[3] D. O. Hebb, *The Organization of Behavior* (Wiley, New York, 1949).

[4] M. A. Nielsen, *Neural Networks and Deep Learning* (Determination Press, 2015).

[5] I. Goodfellow, Y. Bengio, A. Courville, and Y. Bengio, *Deep Learning* (MIT Press, 2016).

[6] N. Caporale and Y. Dan, Spike timing-dependent plasticity: A Hebbian learning rule, Annu. Rev. Neurosci. **31**, 25 (2008).

[7] H. Markram, W. Gerstner, and P. J. Sjöström, A history of spike-timing-dependent plasticity, Front Synaptic Neurosci. **3**, 11 (2011).

[8] D. E. Feldman, The spike-timing dependence of plasticity, Neuron **75**, 556 (2012).

[9] M. A. Nielsen and I. L. Chuang, *Quantum Computation and Quantum Information* (Cambridge University Press, Cambridge, 2010).

[10] P. W. Shor, Algorithms for quantum computation: discrete logarithms and factoring, in *Proceedings 35th Annual Symposium on Foundations of Computer Science*, pp. 124–134 (1994).

[11] D. Deutsch, Quantum theory, the Church-Turing principle and the universal quantum computer, Proc. Royal Soc. Lond. A **400**, 97 (1985).

[12] F. Arute *et al.*, Quantum supremacy using a programmable superconducting processor, Nature (London) **574**, 505 (2019).

[13] E. Pednault, J. A. Gunnels, G. Nannicini, L. Horesh, and R. Wisnieff, Leveraging secondary storage to simulate deep 54-qubit sycamore circuits, arXiv:1910.09534.

[14] A. Peruzzo, J. McClean, P. Shadbolt, M.-H. Yung, X.-Q. Zhou, P. J. Love, A. Aspuru-Guzik, and J. L. O'Brien, A variational eigenvalue solver on a photonic quantum processor, Nat. Commun. **5**, 4213 (2014).

[15] E. Farhi and J. Goldstone, A quantum approximate optimization algorithm, arXiv:1411.4028.

[16] Y. Li and S. C. Benjamin, Efficient Variational Quantum Simulator Incorporating Active Error Minimization, Phys. Rev. X **7**, 021050 (2017).

[17] K. Beer, D. Bondarenko, T. Farrelly, T. J. Osborne, R. Salzmann, D. Scheiermann, and R. Wolf, Training deep quantum neural networks, Nat. Commun. **11**, 808 (2020).

[18] K. H. Wan, O. Dahlsten, H. Kristjánsson, R. Gardner, and M. S. Kim, Quantum generalisation of feedforward neural networks, npj Quantum Inf. **3**, 36 (2017).

[19] J. Romero, J. P. Olson, and A. Aspuru-Guzik, Quantum autoencoders for efficient compression of quantum data, Quantum Sci. Technol. **2**, 045001 (2017).

[20] Y. Cao, G. G. Guerreschi, and A. Aspuru-Guzik, Quantum Neuron: An elementary building block for machine learning on quantum computers, arXiv:1711.11240.

[21] K. Mitarai, M. Negoro, M. Kitagawa, and K. Fujii, Quantum circuit learning, Phys. Rev. A **98**, 032309 (2018).

[22] E. Farhi and H. Neven, Classification with quantum neural networks on near term processors, arXiv:1802.06002.

[23] E. Grant, M. Benedetti, S. Cao, A. Hallam, J. Lockhart, V. Stojevic, A. G. Green, and S. Severini, Hierarchical quantum classifiers, npj Quantum Inf. **4**, 65 (2018).

[24] M. Schuld, A. Bocharov, K. M. Svore, and N. Wiebe, Circuit-centric quantum classifiers, Phys. Rev. A **101**, 032308 (2020).

[25] N. Killoran, T. R. Bromley, J. M. Arrazola, M. Schuld, N. Quesada, and S. Lloyd, Continuous-variable quantum neural networks, Phys. Rev. Research **1**, 033063 (2019).

[26] G. R. Steinbrecher, J. P. Olson, D. Englund, and J. Carolan, Quantum optical neural networks, npj Quantum Inf. **5**, 60 (2019).

[27] L. O. Chua, Memristor - The missing circuit element, IEEE Trans. Circuit Theory **18**, 507 (1971).

[28] L. O. Chua and S. M. Kang, Memristive devices and systems, Proc. IEEE **64**, 209 (1976).

[29] B. Linares-Barranco and T. Serrano-Gotarredona, Memristance can explain Spike-Time-Dependent-Plasticity in Neural Synapses, Nat. Prec. (2009).

[30] D. B. Strukov, G. S. Snide, D. R. Stewart, and R. S. Williams, The missing memristor found, Nature (London) **453**, 80 (2008).

[31] S. H. Jo, T. Chang, I. Ebong, B. B. Bhadviya, P. Mazumder, and W. Lu, Nanoscale memristor device as synapse in neuromorphic systems, Nano Lett. **10**, 1297 (2010).

[32] A. Serb, J. Bill, A. Khiat, R. Berdan, R. Legenstein, and T. Prodromakis, Unsupervised learning in probabilistic neural networks with multi-state metal-oxide memristive synapses, Nat. Commun. **7**, 12611 (2016).

[33] A. Tavanaei, M. Ghodrati, S. R. Kheradpisheh, T. Masquelier, and A. S. Maida, Deep learning in spiking neural networks, Neural Networks **111**, 47 (2019).

[34] K. Roy, A. Jaiswal, and P. Panda, Towards spike-based machine intelligence with neuromorphic computing, Nature (London) **575**, 607 (2019).

[35] J. Gao, L.-F. Qiao, Z.-Q. Jiao, Y.-C. Ma, C.-Q. Hu, R.-J. Ren, A.-L. Yang, H. Tang, M.-H. Yung, and X.-M. Jin, Experimental

Machine Learning of Quantum States, Phys. Rev. Lett. **120**, 240501 (2018).

[36] T. Jones and S. C. Benjamin, QuESTlink – Mathematica embiggened by a hardware-optimised quantum emulator, Quantum Sci. Technol. **5**, 034012 (2020).

[37] D. Querlioz, O. Bichler, P. Dollfus, and C. Gamrat, Immunity to device variations in a spiking neural network with memristive nanodevices, Nanotechnol. IEEE Trans. **12**, 288 (2013).

[38] P. U. Diehl and M. Cook, Unsupervised learning of digit recognition using spike-timing-dependent plasticity, Front. Comput. Neurosci. **9**, 99 (2015).

[39] https://github.com/yingli-gscaep/quantum_memristive_synapses.

[40] S. Sachdev, *Quantum Phase Transition* (Cambridge University Press, 1999).

[41] P. Pfeiffer, I. L. Egusquiza, M. Di Ventra, M. Sanz, and E. Solano, Quantum memristors, Sci. Rep. **6**, 29507 (2016).

[42] J. Salmilehto, F. Deppe, M. Di Ventra, M. Sanz, and E. Solano, Quantum memristors with superconducting circuits, Sci. Rep. **7**, 42044 (2017).

[43] M. Sanz, L. Lamata, and E. Solano, Quantum memristors in quantum photonics, APL Photonics **3**, 080801 (2018).

[44] T. Gonzalez-Raya, J. M. Lukens, L. C. Céleri, and M. Sanz, Quantum memristors in frequency-entangled optical fields, Materials **13**, 864 (2020).

[45] P. Maier, F. Hartmann, T. Mauder, M. Emmerling, C. Schneider, M. Kamp, S. Hfling, and L. Worschech, Memristive operation mode of a site-controlled quantum dot floating gate transistor, Appl. Phys. Lett. **106**, 203501 (2015).

[46] Y. Li, G. W. Holloway, S. C. Benjamin, G. A. D. Briggs, J. Baugh, and J. A. Mol, Double quantum dot memristor, Phys. Rev. B **96**, 075446 (2017).

[47] L. B. Kristensen, M. Degroote, P. Wittek, A. Aspuru-Guzik, and N. T. Zinner, An artificial spiking quantum neuron, npj Quantum Inf. **7**, 59 (2021).